Corrosion Science 141 (2018) 53–62

Contents lists available at ScienceDirect

Corrosion Science

journal homepage: www.elsevier.com/locate/corsci

The corrosion of copper in irradiated and unirradiated humid air

B. Ibrahim[a], D. Zagidulin[a], M. Behazin[c], S. Ramamurthy[a,b], J.C. Wren[a], D.W. Shoesmith[a,b,*]

[a] Department of Chemistry, University of Western Ontario, London, Ontario, Canada
[b] Surface Science Western, University of Western Ontario, London, Ontario, Canada
[c] Nuclear Waste Management Organization, Toronto, Canada

ARTICLE INFO

Keywords:
Copper
Corrosion
Gamma radiation
Copper oxide
Deep geologic repository

ABSTRACT

Copper corrosion in aerated water vapour has been studied as a function of temperature, relative humidity in the presence and absence of a low gamma radiation dose rate. On surface areas covered by a thin water layer corrosion ceased after ≤ 30 days by the formation of CuO on the surface of a Cu_2O layer. At the locations of condensed water droplets corrosion was more extensive since the corrosion product developed porosity. Radiation accelerated the formation of Cu_2O on corroded areas and increased the number and size of the more extensively corroded locations. The distribution of condensed water was the dominant feature controlling corrosion penetration.

1. Introduction

The accepted method for the permanent disposal of spent nuclear fuel in Canada is to bury it in a deep geologic repository (DGR) in a suitable dense intact rock. The fuel will be sealed within a corrosion resistant used fuel container (UFC) and emplaced in boreholes subsequently backfilled with bentonite clay. The chosen UFC involves a dual-walled container fabricated with an inner carbon steel load-bearing vessel and an outer Cu corrosion resistant barrier. To avoid design issues associated with fabrication and welding while taking advantage of the CANDU (CANadian Deuterium Uranium) fuel bundle dimensions, a container with a thin Cu coating on a welded steel vessel is being designed [1].The coating will be applied using commercial processes such as cold spray deposition and electrodeposition [1] and, since the required corrosion allowance is expected to be small, the corrosion performance of coatings with a thickness of a few millimeters are being evaluated [2,3]. Such a design revives the possibility that γ-radiation, emitted by the fuel waste-form, but insignificant for a thick-walled container, could influence the corrosion of the thinner container by producing radiolytic oxidants in the aqueous environment surrounding the container.

After emplacement, containers will experience a sequence of exposure environments as the DGR evolves from the initially disturbed state, when the environment would be warm and oxidizing, to the long term more stable condition, when the environment will be cooler and anoxic. Upon first sealing the repository the temperature at the surface of the containers will rise due to the heat produced by the radioactive decay processes in the fuel. This will produce a low humidity environment in the vicinity of the containers, and negligible corrosion would be anticipated despite the oxidizing conditions. As the containers cool, moisture will return allowing the local relative humidity (RH) to eventually exceed the critical value required to establish aqueous conditions at the container surface and the onset of corrosion [4,5].

As this local re-saturation process proceeds containers will experience a series of exposure conditions which are not necessarily well separated: (1) an early aerated period with no condensed water on the Cu surfaces; (2) a period of aerated vapour in equilibrium with condensed water on the Cu surfaces; (3) a transition period to fully saturated, potentially oxidizing aqueous conditions; and (4) a final aqueous anoxic period after the available O_2 has been consumed by container corrosion and by reactions with minerals and organic matter in the clay [6]. The period required for re-saturation (i.e., the establishment of an RH of 100%) is uncertain but expected to be between 20 and 100 years for a crystalline repository but much longer for a sedimentary clay repository (i.e., > 1000 years) [7]. During this evolution, the redox conditions at the Cu surfaces will be significantly influenced by the γ-radiation fields, which will produce oxidants in both aqueous vapour and condensed water.

The effect of radiation on the corrosion of Cu has been studied in both aqueous solutions [8–11] and in moist air [12,13] but inevitably at radiation dose rates much greater than those expected on a container surface. In both aerated and de-aerated chloride solutions (150 °C, 27 Gy/h) radiation appeared to be beneficial, an apparently protective cuprite (Cu_2O) film being formed [10]. In the absence of radiation, areas of the surface covered with $CuCl_3.3Cu(OH)_2$ were observed and interpreted as indications of more extensive corrosion at locations at

* Corresponding author.
E-mail address: dwshoesm@uwo.ca (D.W. Shoesmith).

https://doi.org/10.1016/j.corsci.2018.05.024
Received 4 December 2017; Received in revised form 23 April 2018; Accepted 23 May 2018
Available online 25 May 2018
0010-938X/

which protection by Cu_2O was lost. At high dose rates (80–770 Gy/h) more extensive corrosion was observed and the deposited corrosion product film (predominantly Cu_2O) was thought to play a significant role in amplifying the influence of γ-radiation [14].

In irradiated moist air, the extent of corrosion damage was found to increase with the moisture content of the gas phase [12,13]. At relatively low dose rates (100 Gy/h (90 °C–150 °C), the influence of radiation was minimal. The estimated corrosion rate was only marginally greater than in the absence of radiation indicating the presence of a protective Cu_2O layer. At higher dose rates (700 Gy/h), cupric nitrate ($CuNO_3(OH)_3$) was formed, indicating more extensive corrosion and the incorporation of radiolytically-produced NO_3^- [15,16,17] at these locations.

In this paper, we describe the results of our studies on the influence of low γ-radiation dose rates on the corrosion of Cu in aerated water vapour at controlled RHs of 70% and 85% and a temperature of 75°C for exposure periods of up to 1 year. These conditions were chosen to simulate the exposure environment anticipated during period 2 (defined above) when the container could be exposed to warm aerated vapour with condensed water on the surface. Experiments were conducted in the presence and absence of radiation fields in an attempt to determine whether low radiation dose rates have any measurable influence on the container corrosion process. Since aerated conditions were maintained for the full duration of the experiments they can be considered conservative, from a waste disposal perspective, since they do not account for the consumption of the limited inventory of oxygen trapped in a DGR on sealing.

2. Experimental

2.1. Materials and their preparation

Coupons were cut from P-deoxidized wrought Cu blocks supplied by the Swedish Nuclear Fuel and Waste Management Company (SKB, Stockholm, Sweden). All coupons were polished successively with 600 and 1200 grit SiC paper on all 6 sides, washed and ultrasonically cleaned in Type I water and methanol for 2 min, and then washed again with Type I water before being dried using ultrapure Ar gas. The polished coupons were placed in a desiccator for one day to dry.

2.2. Experimental procedure

Two sets of experiments were conducted. In one set, the coupons were placed on a Teflon holder with a 1 cm^2 face facing upwards, and the holder then placed in a humidity chamber (Associated Environmental Systems) set to 75 °C and 70% RH. Coupons were removed for analyses after exposure periods of 1, 2, 7, and 14 days and then monthly for up to 1 year. On removal from the chamber, the coupons were dried with Ar gas, and placed in a desiccator for 1 day. Subsequently, they were stored in a glove box to avoid air oxidation prior to analysis using Raman spectroscopy and SEM. A second set of experiments was performed in an oven at 75 °C at Canadian Nuclear Laboratories, Chalk River, Ontario in both the presence and absence of a radiation field. In these experiments the coupons were placed on a Teflon holder with a 1 cm^2 face facing upwards, and the holder placed inside a 1 L glass bottle. A second glass bottle, containing distilled water was cooled to 70 °C, and the humidified air made to flow from this vessel to the test vessel at a flow rate of 50 ml/min to achieve the required 85% RH. One set of coupons was irradiated (using a ^{60}Co γ source) at a dose rate of 0.35 Gy/h, while a second set was shielded from this field behind lead blocks. Coupons were removed after 51 d and 104 d of exposure, having experienced total radiation doses of 425 Gy and 866 Gy, respectively. The radiation dose rates were calculated based on the known activity of the Co-60 source and its distance from the samples. A second measurement was performed in-situ using calibrated ion cambers connected to Keithley electrometers at the exact specimen location and verified by post-experiment analysis using a thermoluminescent dosimeter.

2.3. Analyses of corroded specimens

Raman spectra were acquired using a Renishaw 2000 Raman spectrometer equipped with a He-Ne laser with a wavelength of 632.8 nm used to excite Raman active vibrations. Spectra were recorded over the wavelength range 120-2000 cm^{-1} (some to 4000 cm^{-1}) with the laser power set to 0.5 mW. Spectra were calibrated using the 520.5 cm^{-1} line of a Si wafer. The laser beam was focused onto the sample using a Leica DMLM microscope with a 50x uncoated objective lens.

Micrographs of the Cu coupons were recorded using a Hitachi S4500 Field emission electron microscope (SEM) equipped with an energy dispersive X-ray (EDX) analyzer to collect images and elucidate elemental compositions. SEM micrographs were recorded using an accelerating voltage of 5.0 kV. A Zeiss 1540 XB instrument equipped with a 30 kV Ga ion beam was used to cut focused-ion beam (FIB) cross-sections, and imaging and EDX analyses were performed at an angle of 54°.

X-ray photoelectron spectroscopy (XPS) analyses were performed with a Kratos Axis Ultra spectrometer using an Al Kα monochromatic high energy ($h\upsilon$ = 1486.6 eV) source (15 mA, 14 kV). The instrument work function was calibrated using the Au $4f_{7/2}$ line (BE of 93.95 eV) and the spectrometer dispersion was adjusted using the Cu $2p_{3/2}$ peak with a binding energy (BE) of 932.63 eV. The C 1s peak at 284.8 eV was used as a standard to correct for surface charging. Survey scans were recorded over an area of 300 µm x 700 µm at a pass energy of 160 eV between 0 and 1100 eV. High resolution spectra were obtained for C 1s, O 1s and Cu 2p peaks at a pass energy of 20 eV using a step size of 0.1 eV. Spectral analyses were performed using CasaXPS software (version 2.3.2.4). The Auger parameter was used to confirm the assignment of Cu oxidation states and the type of oxide/hydroxide present. A more detailed description of the analysis of XPS spectra recorded on Cu is given elsewhere [15].

3. Results

3.1. Long-term exposure study (no-radiation)

Specimens from this long-term exposure study exhibited two distinct corrosion features visible in optical images, Fig. 1; (i) general corrosion of the majority of the surface (termed the general area and observed as copper-coloured); and, (ii) a number of apparently more heavily corroded areas (termed patches), seen as purple/blue locations. SEM micrographs of the general areas, recorded after a short exposure period (7 d), Fig. 1, showed a few, small, dispersed globular features. After 120 d of exposure, the surface was covered by a dense, uniform layer of these features. After 360 d a thin layer of oxide covered the general surface with some areas exhibiting larger globular features, consistent with the patchy appearance of the optical images.

Closer inspection of the SEM micrographs recorded on the patches (circled in the optical images), Fig. 1, showed corrosion occurred to a greater extent within the patches than over the general surface. The density of the corrosion product and the size of the features within the patches was consistently larger than in the general area, suggesting more rapid corrosion at these locations. This is thought to be most likely due to surface wetting. These patches of enhanced corrosion appeared to progress along the polishing lines. After prolonged exposure, ≥150 d, an accumulation of bulkier corrosion product was always present within a patch. This appeared as a central dark spot in the optical images.

Comparison of the SEM micrographs in Fig. 1 confirmed that corrosion product accumulated more extensively within the patches. The adsorption of H_2O has been shown to occur more readily on Cu oxides than on Cu at higher humidities [16], with twice as much H_2O adsorbed

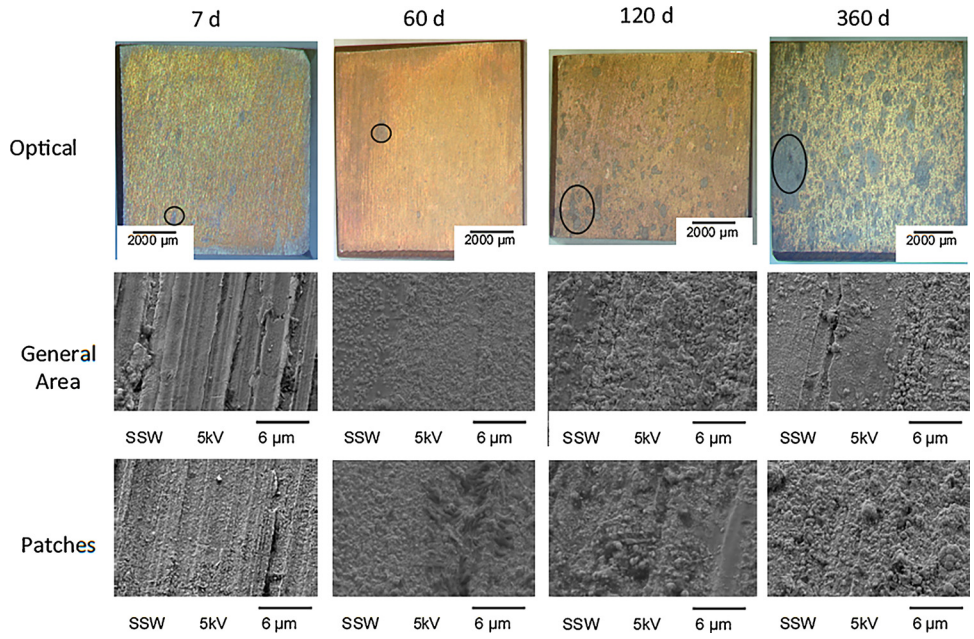

Fig. 1. Optical images and SEM micrographs of samples removed from the humidity chamber after a series of exposure periods. The circles in the optical images indicate the locations shown in the SEM micrographs of the patches.

on Cu_2O as on Cu at an RH of 80%. This was attributed to the higher roughness factor and, hence, the higher surface area of Cu_2O [16], and offers a possible explanation for the enhanced corrosion observed within patches.

XPS analyses, Table 1, showed that the outer most surface of the oxide layer (the top ~ 7 nm) after 7 d of exposure, was a mixture of Cu^{I} and Cu^{II} with Cu^{II} mainly present as $Cu(OH)_2$. The analyses were based on the shape of the Cu 2p spectra compared to standards for Cu, Cu_2O, $Cu(OH)_2$ and CuO [17]. Similar analyses, performed after 90, 180 and 300 d, showed CuO became the dominant phase in the top few nanometers of the surfaces of both the general areas and the patches. Accurately distinguishing between Cu(0) and Cu(I) states in the presence of dominant amounts of Cu(II) is difficult since the Auger spectral lines for these three components overlap [17].

Examples of Raman spectra recorded on multiple surface locations after a number of exposure periods up to 360 d are presented in Fig. 2. Some spectra were distorted by fluorescence at high wavenumbers but distinct peaks were present at wavenumbers < 750 cm^{-1}. After 1 day the spectrum was typical of Cu exposed to air. The peaks present at 147 cm^{-1}, 220 cm^{-1}, and the two peaks at 525 cm^{-1} and 625 cm^{-1}, were assigned to Cu_2O [18–21]. This phase was dominant up to 30 d of exposure, with the peak at 297 cm^{-1}, assigned to CuO, being rarely observed [19,22,23]. After 60 d, the peak at 297 cm^{-1} was commonly observed, especially in the patches. After prolonged exposure, 180–360 d, the peak at 297 cm^{-1} was persistent in spectra recorded on both general areas and patches indicating a general surface coverage by Cu_2O and CuO. After 180 d, the patches generally exhibited a stronger relative intensity for the CuO peak compared to the general areas. This can be seen by comparing the two spectra recorded on a sample exposed for 360 d, which indicate a larger CuO content within the patches than on the general surface. This is consistent with the expectation that patches experienced enhanced surface wetting leading to enhanced oxidation to Cu^{2+}. The Raman analyses did not detect any $Cu(OH)_2$, which would have been seen as a weak peak at ~300 cm^{-1}, and distorted by the presence of CuO, and a strong peak at ~470-490 cm^{-1} [24]. The absence of this strong peak confirmed that CuO was the dominant Cu^{II} phase.

Table 1
Cu oxidation states and phase assignments determined by XPS on several locations on select samples.

	Cu(0) + Cu(I)	Cu(II)	Assignment
7 d – general area	49	51	Cu_2O and $Cu(OH)_2$
7 d – patch	52	48	Cu_2O and $Cu(OH)_2$
90 d – general area	13	87	Mostly CuO
90 d – patch	14	86	Mostly CuO
180 d – general area	6	94	Mostly CuO
180 d – patch	7	93	Mostly CuO
300 d – general area	8	92	Mostly CuO
300 d – patch	8	92	Mostly CuO

Cross-sections, FIB-cut within areas of general corrosion on coupons exposed for 90 d and 150 d, Fig. 3, show the corrosion product layer in these areas was very thin (approximately 99 nm–370 nm).

Similar measurements on a series of coupons exposed for various times, Table 2, showed that the oxide film reached a thickness of 100–200 nm over the first 3 d of exposure and then thickened only marginally with extended exposure periods up to 1 year. Significant variance in thickness was observed which could be partially due to the original surface roughness leading to a non-uniform deposition process. This initially rapid, but eventually very slow, increase in thickness indicated that deposition of the outer CuO layer, detected by both XPS and Raman, inhibited further corrosion.

Film thicknesses measured on a number of patches, Table 3, confirmed that these locations were more heavily corroded than the more general surface, even after only 30 d of exposure. In addition, contrary to the behaviour on general areas, film thicknesses increased with increased exposure (up to 360 d), indicating corrosion continued over the full exposure period. Two patches were cross-sectioned on the sample exposed for 360 d. The thickness of the corrosion product on the smaller patch (in terms of lateral dimensions) ranged from 2.15 µm to 6.09 µm with an average of 4.2 µm, Fig. 4. For the larger patch, thicknesses ranged from ~6.6 µm to 11.7 µm with an average of ~10.5 µm.

For coherent uniform oxide film growth the Pilling-Bedworth ratio (the volume of oxide produced/the volume of metal consumed) can be used to calculate the penetration depth from a measurement of oxide thickness. For Cu_2O this ratio is 1.67 [10]. However, inspection of a number of cross sections showed that the thickness of the corrosion product was very much greater than the apparent depth of metal loss

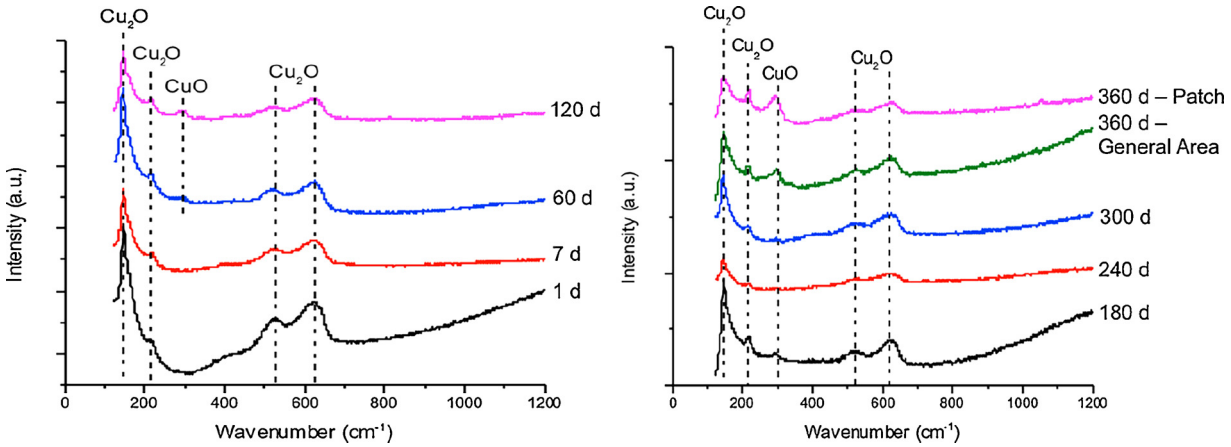

Fig. 2. Raman spectra recorded on Cu coupons after various exposure times. The spectra recorded on the 360 d sample show the increased intensity of the CuO peak (297 cm^{-1}) within a patch compared to the intensity of this peak in spectra recorded on the general area.

within patches. Since, at most, the surface will be covered by only a thin condensed water layer, significant lateral transport of soluble copper was unlikely over macroscopic distances and deposition of corrosion product was likely to have occurred locally. Thus, the presence of a thick layer of oxide over a slightly corroded substrate suggested significant porosity within the deposits. This was confirmed by inspection of the cross sections in Figs. 4 and 5. Consequently, the aspect ratio (the ratio of corrosion product thickness to lateral surface area corroded (indicated in the optical images in Figs. 4 and 5)) can only be considered a qualitative indication of the extent of corrosion. The aspect ratios are extremely small indicating a clear preference for corrosion to spread across, rather than penetrate into, the metal. In addition, the depth of penetration on the patch with the largest surface footprint indicated that corrosion was progressing both laterally and vertically with time.

The distribution of corrosion products was analyzed in detail for the larger patch, Fig. 5. Three distinct layers were observed. The first porous layer had a fairly uniform thickness of ~5.75 µm. The Cu/O ratio, measured by EDX, was large (3.1 to 3.9) suggesting the layer was comprised of Cu_2O. One likely reason for a ratio greater than 2 was that the EDX analysis, performed at an angle and a high accelerating voltage, also detected the Cu substrate. The second more uniform layer, with a thickness of ~850 nm, had a Cu/O ratio of ~1.7, suggesting the presence of a more oxidized Cu state, despite the ratio being close to that expected for Cu_2O. A possibility was that it was a thin layer of CuO formed by the direct oxidation of Cu_2O to CuO by dissolved O_2. The third layer, ~5.12 µm thick, had a more cracked appearance, and a Cu/O ratio of ~1, indicating CuO. This layer also contained up to ~15 at. % of Cl^-. Cl^- was commonly observed and was likely due to its concentration as an impurity in the water over time. Its presence in this layer is likely due to salting out on removing the sample from the humidity chamber, when condensed water would have evaporated leading to the rapid deposition of water soluble ions on the surface. Samples exposed for only 90 and 150 d showed similar variations in the Cu/O ratios but the outer layer was considerably thinner, at ~0.8 and 3 µm,

Table 2
Thickness of the general corroded area after various exposure times in the absence of radiation. The thickness is an average of 10 measurements taken across each cross-sectional area.

Time (d)	Thickness (nm)	Stdev (nm)
30	169.77	110.07
90	162.80	64.85
150	365.88	248.55
360	240.00	134.12

Table 3
Thickness of the corrosion product accumulated in a patch after various exposure times in the absence of radiation. The thickness is an average of 10 measurements taken across each cross-sectional area.

Time (d)	Thickness (µm)	Stdev (µm)
30	0.53	0.17
90	1.20	0.56
90	0.83	0.35
90	0.63	0.19
150	1.81	0.80
150	3.89	1.79
360	4.23	1.52
360	10.51	2.55

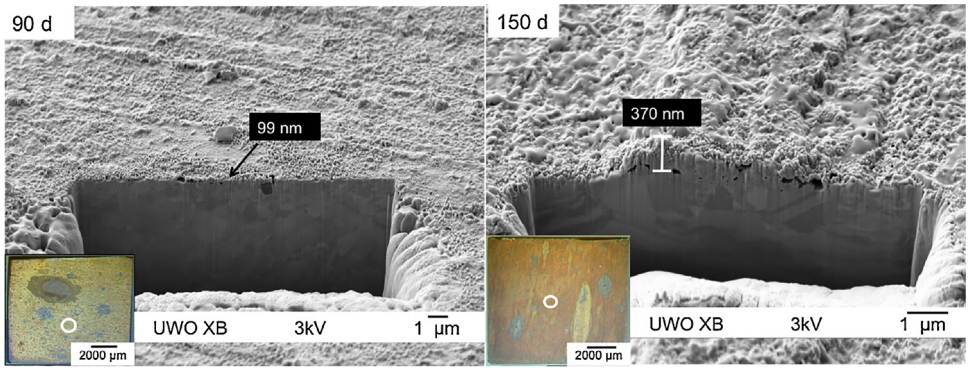

Fig. 3. FIB cut cross-section of the general area on the 90 and 150 d samples at the locations indicated by the white circle in the optical images.

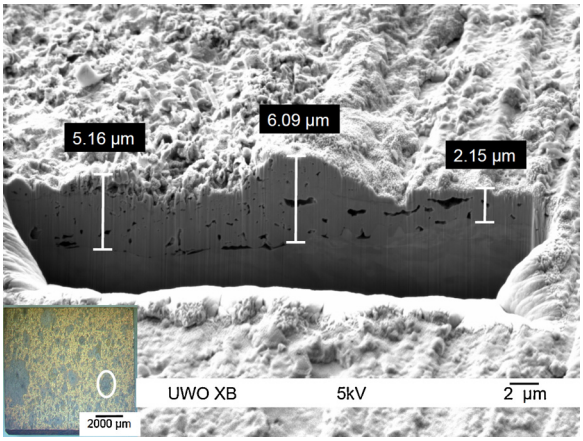

Fig. 4. FIB-cut cross-section of the small patch on the 360 d exposed sample indicated by the white circle in the optical image. The cross-section shows the variance in corrosion product thickness across a portion of the patch.

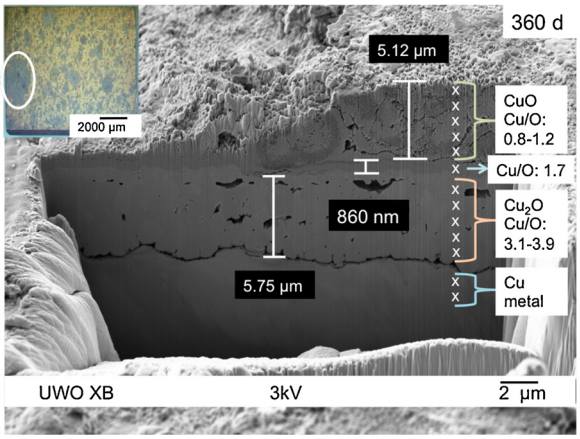

Fig. 5. FIB cut cross-section of the large patch on the 360 d exposed sample indicated by the white circle in the optical image. The cross-section shows three distinct layers, an initial, compact layer of Cu_2O, a second intermediate layer with a Cu to O ratio of 1.7, and a third, more cracked layer of CuO deposited on top. The locations at which EDX spot scans were performed are marked with an X.

respectively. These observations were consistent with an increased accumulation of CuO with exposure time on the Cu_2O layer deposited on the Cu surface, and confirmed that corrosion was on-going within patch areas.

For the pH range likely to prevail in these experiments (6 to 8) Cu^{2+} ions were more soluble than Cu^{+} ions and the most likely to have dissolved into the small volume of water on the surface [25,26]. In the thin film of condensed H_2O, the solubility limit was likely reached very quickly, leading to the onset of both Cu_2O and CuO deposition. The continued growth of the Cu_2O layer as a function of time, as demonstrated by the increasing thicknesses, Table 3, indicated that, within the patches, the deposition of CuO did not block the surface from further corrosion, as observed for general areas. Corrosion at the Cu surface and transport of soluble Cu through water filled pores (seen to be present in the deposit) could have maintained the on-going deposition at the outer surface leading to the build-up of the thickening CuO layer.

3.2. The effect of low dose radiation on Cu corrosion

In the presence of a low γ-radiation dose rate similar corrosion features were observed; (i) the general corrosion of the majority of the surface (Cu coloured in optical images); and, (ii) more extensively corroded patches (blue/purple in optical images), Fig. 6. After 51 d of exposure the general areas of the irradiated surfaces appeared slightly more corroded than non-irradiated surfaces. After 104 d both surfaces were covered with a layer of nodular deposits, which were larger on the irradiated than on the non-irradiated surface, indicating accelerated corrosion.

FIB-cut cross sections (not shown) showed the surface films on the general areas of unirradiated specimens were ~100 to ~300 nm thick after 104 d, consistent with the values in Table 2. On irradiated surfaces the films were ~70 to ~ 200 nm thick. These latter values were in line with published studies, which reported similar thicknesses after several days of exposure to a non-irradiated environment with a similar RH but lower temperature [13]. The absence of any increase in thickness with extended exposure times in the presence of γ-radiation, despite the more rapid initial growth, suggested low levels of radiation may be beneficial in producing a coherent protective Cu_2O/CuO layer.

Inspection of the optical images, Fig. 7, showed the darker patches on the irradiated coupon covered a larger area of the surface after the longer exposure period with their growth having progressed predominantly along the polishing lines in the surface. An influence of γ-radiation on the size of the patches was observed, the irradiated surface possessing a greater number of patches after both exposure periods, Fig. 7. Their areal dimensions were also greater suggesting their lateral growth may have been accelerated by the presence of irradiation, possibly due to the local generation of radiolytic oxidants.

The SEM micrographs, Fig. 7, showed that, compared to the general surface, corrosion within the patches led to denser more copious corrosion product within these locations. In addition, corrosion appeared more extensive with a greater number of larger patches in the presence of radiation, Fig. 7. Additionally, the corrosion product formed larger nodules, suggesting a faster growth rate in the presence of radiation.

As observed in the absence of radiation (Figs. 4 and 5), a FIB cut cross section of a corroded patch confirmed that the extent of corrosion was greater at these locations than on the general surface, Fig. 8. Inspection of the Cu/oxide interface showed that, despite these variations in film thickness the differences in penetration depths into the Cu were minor demonstrating that corrosion was leading to a “polishing” effect at this location. A section cut from a second patch exhibited a much thicker deposit (7.7 to 9.7 µm) indicating considerable variations in local corrosion rates. For the first specimen (Fig. 8) additional FIB cuts (not shown) were made at locations 50 µm outside and inside the edge of a patch, which showed that the film thickness varied from ~60 nm to ~170 nm outside the patch (i.e., on the generally corroded surface) to ~160 nm to ~390 nm just inside the edge.

This last observation suggested that corrosion within a patch was more extensive at the center (Fig. 8) than close to the periphery, irrespective of whether the specimen was irradiated. This was confirmed by examining a cross section cut through the central mass of corrosion product on a non-irradiated specimen (after 104 days of exposure), Fig. 9. A number of features were noteworthy: (i) a shallow penetration into the Cu was observed, (ii) the depth of penetration was not necessarily beneath the thickest deposit; and (iii) considerable void space existed within the deposit. The second two observations indicated the importance of transport, at least locally, of soluble Cu^{2+}, confirming that a significant volume of condensed water was present at this location. The concentration of corrosion at such locations suggested that the condensation of aerated H_2O was the dominant factor promoting corrosion at local sites not the presence of γ-radiation.

EDX analyses were performed on a number of cross sections where the distribution of corrosion products was found to be similar. The results obtained from analysis of the cross section shown in Fig. 9 are tabulated in Table 4. The Cu/O ratios varied from 2.25 (location 1) to 4.1 (location 2) and 3.7 (location 3) confirming the film was dominantly Cu_2O. The high ratios at locations 2 and 3 could be attributed to the simultaneous detection of the Cu substrate. No O signal was detected at location 4 confirming the location of the Cu/Cu_2O interface. Raman spectra recorded on the general surface and on patches on both

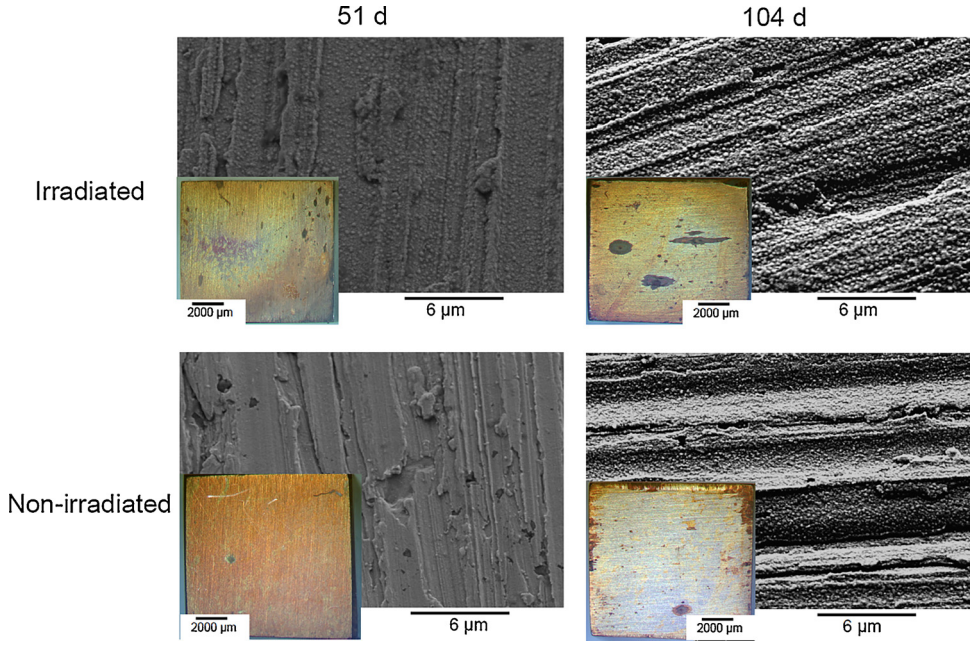

Fig. 6. SEM micrographs of the surfaces of coupons exposed for different times showing corrosion of the general areas (Cu-coloured) in the corresponding optical images.

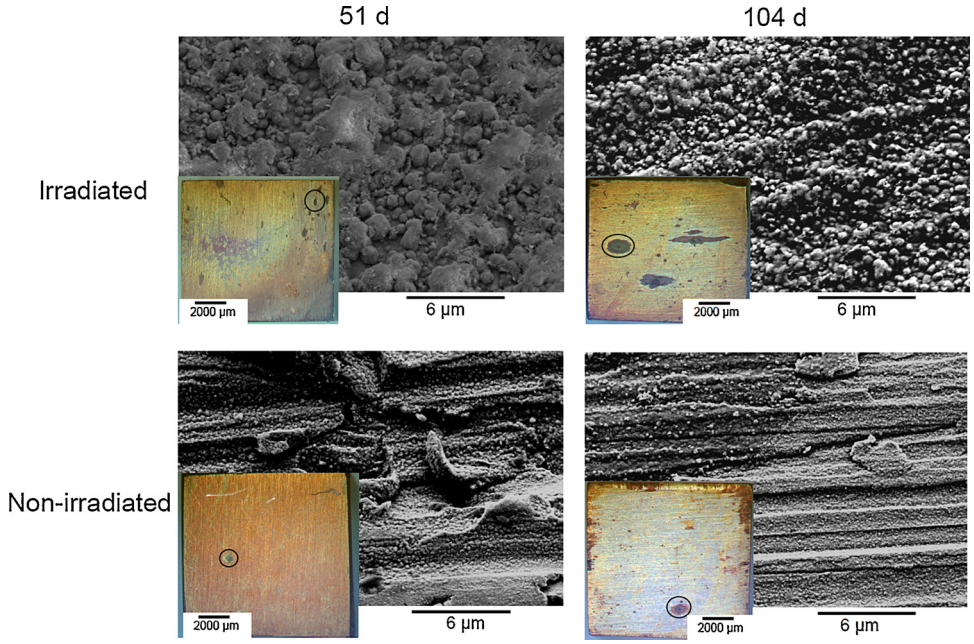

Fig. 7. SEM micrographs of the surfaces of coupons for different exposure times showing the corrosion within the patches marked with circles in the optical images.

irradiated and non-irradiated specimens showed the presence of both Cu_2O and CuO. No N-species were detected on irradiated specimens despite the likely presence of radiolytically-formed HNO_3. Although a more extensive analysis of corroded patches is required there was no evidence in the present study that the low radiation dose rate employed lead to deeper corrosion penetration into the metal.

4. Discussion

The majority of the Cu surface, the general area, was rapidly covered by a uniform Cu_2O film. In the absence of radiation, O_2 reduction would have been the main cathodic reduction reaction supporting corrosion

$$O_2 + 4H_2O + 4e^- \rightarrow 4OH^-. \quad (1)$$

When radiation was present, H_2O_2 reduction (the dominant molecular oxidant produced by the gamma radiolysis of water) would also have contributed

$$H_2O_2 + 2e^- \rightarrow 2OH\text{-} \quad (2)$$

and in irradiated air there was also the possibility of HNO_3 reduction

$$NO_3^- + 8e^- + 9H^+ \rightarrow 3H_2O + NH_3. \quad (3)$$

Under non-irradiated conditions and at low γ-dose rates, O_2 reduction was expected to be the dominant cathodic reaction since the transport path from the solution/vapour interface, at which O_2

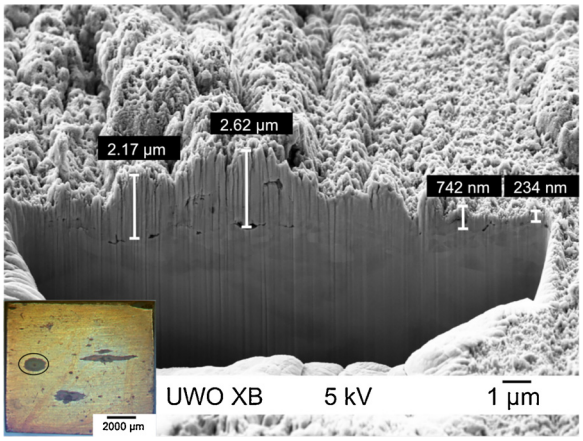

Fig. 8. A FIB cut cross section of an irradiated sample exposed for 104 d. The section was cut from within the circled area shown in the optical image.

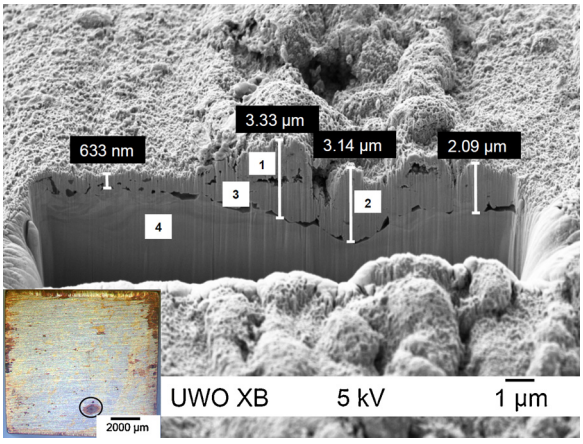

Fig. 9. A FIB cut cross section on a non-irradiated sample exposed for 104 d. The section was cut from within the circled area shown in the optical image. The numbers in the SEM micrograph indicate the locations analyzed by EDX (Table 4).

Table 4
EDX data recorded on the cross-section of a patch on a non-irradiated sample after 104 days of exposure. The locations analyzed are numbered in Fig. 9.

	C K (at. %)	O K (at. %)	Cl K (at. %)	Cu L (at. %)
Spot 1	7.9	28.1	1.0	63.0
Spot 2	12.1	16.8	1.5	69.6
Spot 3	13.4	18.0	1.1	67.4
Spot 4	8.00	–	–	92.0

absorbed into solution, to the corroding surface was short.

While O_2 was readily available, its ability to support Cu corrosion was dependent on the nature of the surface film. Initially its reduction occurred on the bare metal surface to produce Cu^{I} and possibly Cu^{II} adsorbed states,

$$Cu \rightarrow (Cu^{I})_{ads} \rightarrow (Cu^{II})_{ads} \quad (4)$$

Irrespective of the nature of the adsorbed state, the subsequent dissolution of Cu would be predominantly as Cu^{2+} which is considerably more soluble in the prevailing pH range (6–8) [25,26]. Even if dissolution occurred as Cu^{+} its homogeneous oxidation to Cu^{2+} would be expected [27]

$$4Cu(I) + O_2 + 2H_2O \rightarrow 4Cu(II) + 4OH^{-} \quad (5)$$

Given the limited amount of condensed H_2O available, saturation by Cu^{2+} would be rapidly approached. Depending on the initial pH, hydrolysis of Cu^{2+} could have been initially very limited leading to an increase in pH as OH^{-} accumulated (reactions (1)–(3)). This increase would be rapidly arrested by the formation of hydrolyzed species such as $Cu(OH)^{+}$ and $Cu_2(OH)_2^{2+}$ [28]. Since the solubility of Cu^{2+} is limited (between 10^{-5} and 10^{-8} mol/L in this pH range) $Cu(OH)_2$ could have separated as colloidal particles [28] and precipitated on the Cu surface probably in gelatinous form [29,30].

As discussed elsewhere, the formation of Cu_2O then occurred by the subsequent reduction of $Cu(OH)_2$ via galvanic coupling to the substrate Cu

$$Cu(OH)_2 + Cu \rightarrow Cu_2O + H_2O \quad (6)$$

with Cu_2O initially forming a nodular deposit, which rapidly became compact eliminating the galvanic couple by blocking the anodic dissolution of the Cu substrate. A small fraction of the $Cu(OH)_2$ could have been converted to CuO, as observed after longer exposure periods (Table 1), leading to the passivation of the Cu in the general areas on the surface. It is also possible in this pH range that direct oxidation of the Cu_2O by dissolved O_2

$$2Cu_2O + O_2 \rightarrow 4CuO \quad (7)$$

also contributed to the formation of the insulating outer layer. The formation of a compact Cu_2O layer and an insulating outer layer of CuO would have blocked both the anodic metal dissolution and O_2 reduction reactions and prevented further corrosion. Estimates of the thickness in the general areas of the surface showed this occurred after ~30 d, a period over which Raman spectroscopy and XPS demonstrated the presence of a layer of CuO on the outer surface of the Cu_2O layer (Table 1). A schematic of the corrosion process illustrating the key reaction steps proposed is shown in Fig. 10.

The effect of a low γ-dose rate on corrosion in the general areas appeared marginal. The initial rate of coverage by Cu_2O nodules appeared to have been accelerated, but over an extended exposure period the thickness of the corrosion product deposit in the presence of radiation was comparable to that in the absence of radiation, Fig. 11.

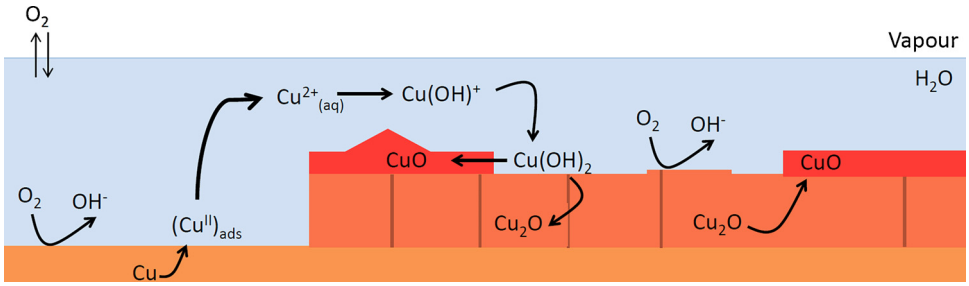

Fig. 10. Illustration of uniform corrosion occurring in a small water volume on the general surface area of the Cu coupons. Bold arrows indicate fast processes. The vertical lines in the Cu_2O layer indicate boundaries between nodules.

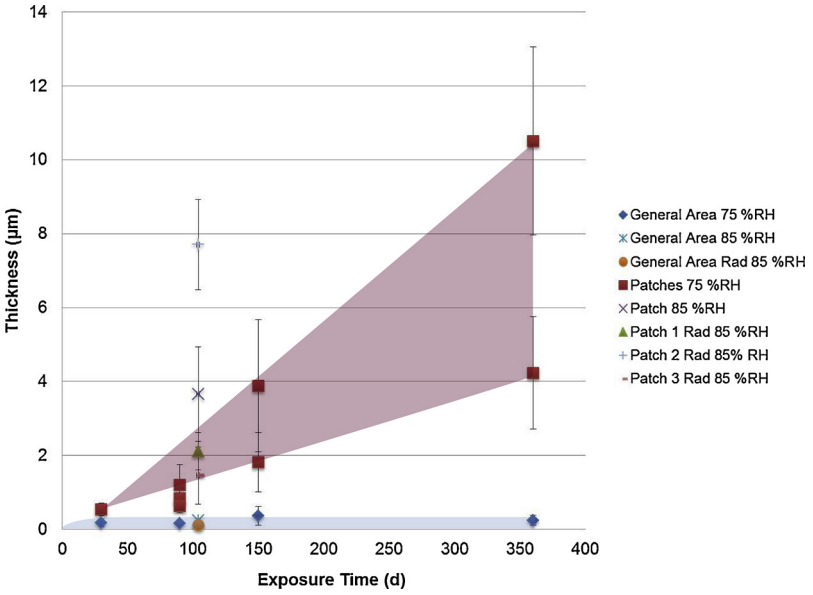

Fig. 11. The effect of exposure time on the thickness of corrosion product deposits on the general area and within patches, based on data from both the long-term study and the low dose γ-radiation study. The blue (lower) block shows that beyond the initial rapid increase of the general area thickness, the thickness does not increase with increasing exposure time. The red (upper triangle) block shows that the thickness within the patches increases with increasing exposure time. (For interpretation of the references to colour in this figure legend, the reader is referred to the web version of this article).

Raman spectroscopy confirmed the surface was covered by CuO after 51 d exposure to radiation, but there was insufficient data to determine whether radiation had any influence on the amount of CuO present. Based on these analyses radiation appeared to play two roles; (i) it induced a more rapid wetting of the surface probably due to the deliquescent nature of HNO_3 [31,32]; and (ii) it produced highly oxidizing species leading initially to an acceleration of corrosion by increasing the rate of formation of Cu^I and, consequently, a more rapid accumulation of Cu_2O nodules on the Cu surface. Beyond these initial effects there was no confirmed additional effect of radiation on the general corrosion process.

The areas of the surface which exhibit more crystalline and thicker corrosion product deposits (termed patches) were likely locations on which water condensed in droplet form (discussed above) as opposed to forming just a thin layer as in the general areas of the surface. Examination of the deposits showed they were porous with a low density, the thickness of the corrosion product deposit being much greater than the local depth of penetration into the Cu. The long-term study in the absence of radiation showed that the corrosion product at these locations did not necessarily achieve a limiting thickness but continued to thicken with exposure time.

The larger volume of H_2O condensed at these locations allowed the sequence of reactions leading to Cu_2O formation to continue without the immediate deposition of dissolved Cu^{2+}. On-going corrosion in this manner led to porosity in the Cu_2O layer as indicated by the eventual accumulation of thick surface layers of Cu_2O, and eventually CuO. This development of porosity could be attributed to the oxidation of Cu_2O most likely at particle boundaries in the initially formed Cu_2O layer,

$$Cu_2O + O_2 + 3H_2O \rightarrow 2Cu(II) + 6OH^-. \quad (8)$$

When this occurred, oxidants in particular dissolved O_2, but also radiolytic oxidants, had access to and reacted on the Cu surface. This porosity was also likely to retain H_2O maintaining the conditions required for corrosion to progress. With the cathodic reaction localized within these pores a significant increase in pH would have occurred as a consequence of OH^- production due to O_2/H_2O_2 reduction. This would have increased the solubilities of both Cu^{2+} and Cu^+ and provided the concentration gradient required for their transport out of the pores. In the oxidizing environment existing within the pores, transport as Cu^+ was very unlikely despite the increases in its solubility. Encountering more neutral conditions beyond the pores would have caused a decrease in solubility and the deposition of $Cu(OH)_2$ leading to Cu_2O formation via the sequence of reactions described above. These deposition processes did not block this porous structure and the dual layer continued to thicken with the surface remaining active. Fig. 12 attempts to illustrate this reaction sequence. The inability of CuO to passivate the surface within the patches was consistent with the observations that the deposited CuO only partially covered the surface. Additionally, by allowing corrosion to continue at the Cu surface it was also possible that some degradation of the Cu/Cu_2O interface occurred accounting for the void space at many interfacial locations within the patches.

The influence of low γ-dose rates on this process could have been counterbalancing. The formation of more aggressive oxidants could have enhanced the onset of porosity (via reaction (8) (but involving H_2O_2 rather than O_2) thereby increasing the number of patches. However, by simultaneously accelerating the formation of Cu^{2+}, the solubility of CuO would have been exceeded more rapidly causing a limitation in the thickening of the dual layer deposit.

The number and lateral spread of corrosion patches appeared to increase with exposure time and to be enhanced by the low radiation dose rate although there was no evidence that the depth of corrosion within a patch was enhanced by radiation. This observation suggested that the distribution of condensed water was the dominant feature controlling the development of patches, a process possibly enhanced by the production of deliquescent HNO_3 by the radiolysis of H_2O vapour. The spreading of patches with time indicated that lightly corroded general areas of the surface were reactivated, FIB-cut cross sections cut at the border between patches and the generally corroded areas of the surface showing a gradual transition in the thickness of the deposit.

It has been claimed [14,33] that the influence of gamma radiation on Cu corrosion is significantly enhanced by the presence of Cu_2O/CuO films, due to the catalytic ability of Cu and its oxides to produce reactive radicals (such as $OH^{\bullet}$). At the dose rates employed in this study it is likely that the main influence of radiation, in slightly promoting the growth of patches, is its production of H_2O_2. The direct reaction of H_2O_2 (via its decomposition to produce $OH^{\bullet}$) with Cu causing corrosion is thought to be minimal once an oxide is formed [34]. However, in the porous oxides obtained in the present study, the confinement of H_2O_2 within the porous structure would allow it to act as a cathodic reagent promoting Cu corrosion at exposed locations at the base of pores. As demonstrated, this effect appears minor at the low dose rates employed.

A secondary spreading of condensed H_2O droplets has been observed in atmospheric corrosion studies and attributed [35] to a slight enhancement of cathodic activity at the periphery of the droplet. It was claimed that the alkalinity produced by O_2 reduction (reaction (1)) led

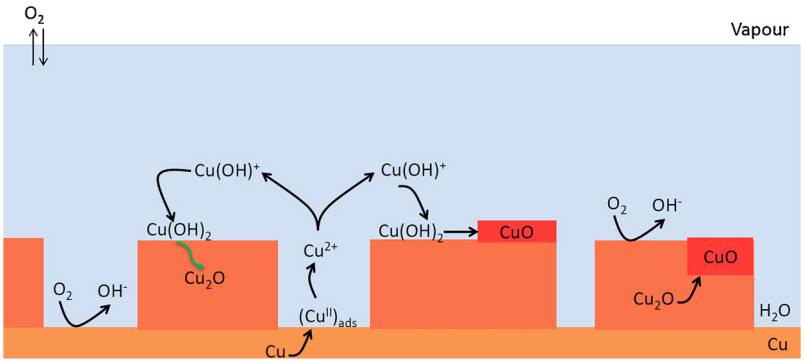

Fig. 12. Illustration of the corrosion process occurring within patches in a large water volume. The gaps between the Cu_2O nodules are exaggerated to facilitate illustration of the reaction steps.

to a lowering of surface tension at the H_2O/oxide interface which allowed the H_2O droplet to spread. This enhanced alkalinity would enhance the solubility of Cu^{2+} via hydrolysis

$$Cu^{2+} + xOH^- \rightarrow Cu(OH)_x^{(2-x)-}. \quad (9)$$

This combination of enhanced wetting and increased Cu^{2+} solubility could have been sufficient to reactivate the periphery of a patch leading to further corrosion and spreading of the patch.

5. Summary and conclusions

Corrosion of Cu in both non-irradiated and irradiated aerated H_2O vapour led to two different areas of corrosion: (i) a generally corroded surface on areas covered by a thin H_2O layer; and (ii) a number of more heavily corroded areas (patches) at locations of condensed H_2O droplets.

The corrosion product layer on the generally corroded areas reached a limiting thickness after $\leq$ 30 d and did not measurably thicken over the subsequent exposure period of up to 360 d. This was attributed to the passivation of the surface by an insulating CuO deposit formed on a rapidly grown Cu_2O layer, which blocked both the anodic and cathodic reactions.

Low γ dose rates exhibited only a marginal influence on generally corroded areas, leading to the more rapid wetting of the surface and formation of Cu_2O nodules. No measurable increases in oxide layer thickness were detectable over extended exposure periods.

In the larger volumes of H_2O condensed in patches the Cu_2O remained porous and the CuO eventually deposited did not lead to passivation allowing corrosion to continue and the corrosion product layer to thicken over the extended 360 d exposure period.

The depth of corrosion penetration into the Cu was relatively minor compared to the rate of lateral spread of patches across the surface.

The number and lateral spread of corrosion patches appeared to increase with exposure time and to be enhanced by the low γ dose rate although there was no evidence that radiation increased the depth of corrosion penetration.

The distribution of condensed H_2O appeared to be the dominant feature controlling the development of patches.

Acknowledgements

This project was funded under a collaborative research and development grant funded by the Canadian Natural Sciences and Engineering Research Council (NSERC) and the Nuclear Waste Management Organization (Toronto, Canada). We would like to thank Jared Smith for designing the low-dose radiation experiment at CNL and Jamie Noël for help in setting up the experiment; Todd Simpson (Western Nanofabrication Laboratory) for assistance in obtaining FIB cut cross-sections; and Mark Biesinger (Surface Science Western) for assistance with XPS analyses.

References

[1] P.G. Keech, P. Vo, S. Ramamurthy, J. Chen, D.W. Shoesmith, Design and development of copper coatings for the long term storage of used nuclear fuel, Corros. Eng. Sci. Technol. 49 (2014) 425–430.
[2] R. Partovi-Nia, S. Ramamurthy, D. Zagidulin, J. Chen, R. Jacklin, P. Keech, D.W. Shoesmith, Corrosion of cold spray deposited copper coatings on steel substrates, Corrosion 71 (2015) 1237–1247.
[3] T. Standish, J. Chen, R. Jacklin, P. Jakupi, S. Ramamurthy, D. Zagidulin, P. Keech, D.W. Shoesmith, Corrosion of copper-coated steel high level nuclear waste containers under permanent disposal conditions, Electrochim. Acta 211 (2016) 331–342.
[4] C. Leygraf, Atmospheric corrosion, in: P. Marcus, J. Oudar (Eds.), Corrosion Mechanisms in Theory and Practice, Marcel Dekker, New York, 2000.
[5] C. Leygraf, T.F. Graedel, Atmospheric Corrosion, Wiley Interscience, New York, 1995.
[6] F. King, C. Lijia, K. Pederson, P. Pitkanen, M. Vahanen, An Update of the State-of-the-Art Report on the Corrosion of Copper Under Expected Conditions in a Deep Geologix Repository; TR-10-67, The Swedish Nuclear Fuel and Waste Management Organization (SKB), 2010.
[7] F. King, D.S. Hall, P.G. Keech, Nature of the near-field environment in a deep geological repository and the implications for the corrosion behavior of the container, Corros. Eng. Sci. Technol. 52 (2017) 25–30.
[8] D.W. Shoesmith, F. King, The Effects of gamma Radiation on the Corrosion of Candidate Materials for the Fabrication of Nuclear Waste Packages, AECL-11999; Atomic Energy of Canada Limited, 1999.
[9] F. King, C.D. Litke, The Corrosion Of Copper in Synthetic Groundwater at 150(O) C. Part I The Results Of Short Term Electrochemical Tests, TR-428; Atomic Energy of Canada Limited, 1987.
[10] F. King, C.D. Litke, K.J. George, The Corrosion Of Copper in Synthetic Groundwater at 150(O) C. Part II The Characteization Of Surface Films, TR-464; Atomic Energy of Canada Limited, 1989.
[11] J.P. Simpson, Experiments on Container Materials for Swiss High Level Waste Disposal Projects; Part II: National Cooperative for the Disposal of Radioactive Waste, TR 84-01; Nagra, 1984.
[12] D.T. Reed, V. Swayambunathan, B.S. Tani, R.A. Van Konynenburg, Corrosion product identification and relative rates of corrosion of candidate metals in an irradiated air-steam environment, Proc. Mater. Res. Soc. Symp. 176 (1989) 517–524.
[13] D.T. Reed, R.A.V. Konynenburg, Corrosion of copper-base materials in irradiated moist air systems, Proc. Mater. Res. Soc. Symp. 212 (1991) 317–325.
[14] A. Björkbacka, C.M. Johnson, C. Leygraf, M. Jonsson, Role of the oxide layer in radiation-induced corrosion of copper in anoxic water, J. Phys. Chem. C 120 (2016) 11450–11455.
[15] M.C. Biesinger, Advanced analysis of copper X-ray photoelectron spectra, Surf. Interface Anal. 49 (2017) 1325–1334.
[16] S.P. Sharma, Adsorption of water on copper and cuprous oxide, J. Vac. Sci. Technol. 16 (5) (1979) 1557–1559.
[17] M.C. Biesinger, L.W.M. Lau, A.R. Gerson, R.S.C. Smart, Resolving surface chemical states in XPS analysis of first row transition metals, oxides and hydroxides: Sc, Ti, V, Cu and Zn, Appl. Surf. Sci. 257 (2010) 887–898.
[18] P. Ropret, T. Kosec, Raman investigation of artificial patinas on recent bronze – part I: climatic chamber exposure, J. Raman Spectrosc. 43 (11) (2012) 1578–1586.
[19] R.L. Frost, Raman spectroscopy of selected copper minerals of significance in corrosion, Spectrochim. Acta Part A 59 (6) (2003) 1195–1204.
[20] R.L. Frost, W. Martens, J.T. Kloprogge, P.A. Williams, Raman spectroscopy of the basic copper chloride minerals atacamite and paratacamite: implications for the study of copper, brass and bronze objects of archaeological significance, J. Raman Spectrosc. 33 (10) (2002) 801–806.
[21] F. Texier, L. Servant, J.L. Bruneel, F. Argoul, In situ probing of interfacial processes in the electrodeposition of copper by confocal Raman microspectroscopy, J. Electroanal. Chem. 446 (1) (1998) 189–203.

[22] J.C. Hamilton, J.C. Farmer, R.J. Anderson, In situ raman spectroscopy of anodic films formed on copper and silver in sodium hydroxide solution, J. Electrochem. Soc. 133 (4) (1986) 739–745.
[23] H. Hagemann, H. Bill, W. Sadowski, E. Walker, M. Francois, Raman spectra of single crystal CuO, Solid State Commun. 73 (6) (1990) 447–451.
[24] G. Niaura, Surface-enhanced Raman spectroscopic observation of two kinds of adsorbed OH- ions at copper electrode, Electrochim. Acta 45 (2000) 3507–3519.
[25] D.A. Palmer, Solubility measurements of crystalline Cu_2O in aqueous solution as a function of temperature and pH, J. Solut. Chem. 40 (2011) 1067–1093.
[26] C.F.J. Baes, R.E. Mesmer, The Hydrolysis of Cations, Robert E. Kreiger Publishing Company Inc, New York, N. Y, 1976.
[27] V. Sharma, F.J. Millero, The oxidation of Cu(I) in electrolyte solutions, J. Solut. Chem. 17 (1988) 581–598.
[28] L. Durand-Keklikian, E. Matijevic, Needle-type colloidal copper (II) hydroxide particles, Colloid Polym. Sci. 268 (1990) 1151–1158.
[29] H.W. Richardson, Handbook of Copper Compounds and Applications, Marcel Dekker Inc., New York, 1997.
[30] L. Pauling, General Chemistry, 3rd ed., W.H. Freeman, San Francisco, 1970.
[31] F. Samie, J. Tidblad, V. Kucera, C. Leygraf, Atmospheric corrosion effects of HNO_3—Influence of concentration and air velocity on laboratory-exposed copper, Atmos. Environ. 40 (2006) 3631–3639.
[32] F. Samie, J. Tidblad, V. Kucera, C. Leygraf, Atmospheric corrosion effects of HNO_3—Influence of temperature and relative humidity on laboratory-exposed copper, Atmos. Environ. 41 (2007) 1374–1382.
[33] A. Björkbacka, C.M. Johnson, C. Leygraf, M. Jonsson, Radiation induced corrosion of copper in humid air and Ar atmospheres, J. Electrochem. Soc. 164 (2017) C201–C206.
[34] A. Björkbacka, M. Yang, C. Gasparrini, C. Leygraf, M. Jonsson, Kinetics and mechanism of reactions between H2O2 and copper and copper oxides, Dalton Trans. 44 (2015) 16045–16051.
[35] Z.Y. Chen, D. Persson, A. Nazaroc, S. Zakipour, D. Thierry, C. Leygraf, In situe studies of the effect of CO_2 on the initial NaCl-induced atmospheric corrosion of copper, J. Electrochem. Soc. 159 (9) (2005) B342–351.